J. Fluid Mech. (1987), *vol.* 183, *pp.* 77–94
Printed in Great Britain

Stability of Bödewadt flow

By ÖMER SAVAŞ

School of Aerospace, Mechanical and Nuclear Engineering
The University of Oklahoma, Norman, OK 73019, USA

(Received 6 April 1986 and in revised form 18 February 1987)

Boundary-layer transition over a stationary disk in rotating flow is studied experimentally. Circular waves are observed in the boundary layer occurring on an end disk of a cylindrical cavity during impulsive spin-down to rest. The transient flow evolves into a quasi-steady regime that exhibits the properties of the Bödewadt flow. The circular waves develop in that flow. The critical Reynolds number $Re = r(\Omega/\nu)^{\frac{1}{2}}$ is determined from frequency and wavelength measurements to be about 25. The corresponding dimensionless wavenumber $2\pi r/\lambda Re$ is about 0.6 and the frequency $2\pi f/\Omega_i Re$ about 0.2.

1. Introduction

Steady flows over a rotating infinite disk in a rotating flow have been studied theoretically when both the disk and the fluid over it are rotating in the same direction (Kármán 1921; Bödewadt 1940; Rogers & Lance 1960). The range extends from quiescent flow over a rotating disk (Kármán flow) to rotating flow over a stationary disk (Bödewadt flow). Zandbergen & Dijkstra (1977) and Lentini & Keller (1980) have extended the solutions beyond the Kármán flow to where the disk is rotating faster than the fluid far above it and in the opposite sense. The velocity profiles within the boundary layer over the disk are non-monotonic and prone to various modes of instabilities. Two such modes, both spiral, commonly known as Type I (Class B) and Type II (Class A) waves, were investigated by Gregory, Stuart & Walker (1955), Faller (1963), Faller & Kaylor (1966, 1967), Tatro & Mollo-Christensen (1967), and more recently by Wilkinson & Malik (1985). Type I waves have a well-defined orientation with respect to the azimuthal flow direction. They are at about 15° toward the centre of the disk from that direction. Type II waves have longer wavelengths than Type I waves and may be oriented either toward or away from the centre. Type I waves may be thought of as an intrinsic instability mode of the secondary flow near the wall due to the rotation of the boundary layer with respect to the fluid over it. In this respect, the instabilities observed experimentally on a rotating disk (Faller 1963), on a rotating cone (Kobayashi & Izumi 1983; Kobayashi, Kohama & Kurosawa 1983), and on rotating axisymmetric bodies (Kegelman, Nelson & Mueller 1983; Kohama 1985; Kohama & Kobayashi 1983) belong in the category of Type I (Class B) waves. These instability waves roll-up into spiral vortices close to the wall. They break down eventually and contribute to transition to turbulence in the boundary layer. Visualization experiments of Clarkson, Chin & Shacter (1980) have provided further data on the nature of Type I instabilities, even though they could not identify Type II instabilities in their experiments. During their investigations of the transition of the flow between rotating disks, Szeri *et al.* (1983) reported a type of instability that occurs in irregular patterns. The structure

is concentric on the average and is identified as Type II waves. Neither an experimental nor a theoretical study of the stability of the Bödewadt flow seems to be currently available.

Boundary-layer-stability experiments are usually done in steady-flow apparatus where there is no time constraint during probing into the flow as the turbulent fluids resulting from the breakdown of the instability waves are washed downstream continually. The laminar–turbulent transition in the boundary layer on a flat plate is a familiar flow of this type. Rotating-flow experiments where the secondary flows on the surfaces progress from the stable regions of the flow to the unstable regions also enjoy this convenience. The Kármán flow and its variations, such as the flow over a rotating cone, constitute one such class of flows. The Bödewadt flow, by contrast, poses serious difficulties for laboratory study. Conceptually, that the fluid moving from infinity through the viscous boundary layer emerges intact into the inviscid interior seems to run against the conventional unmediated perception of viscous flows (Greenspan 1968, p. 138). Experimentally, the stability characteristics of the viscous layer are uncertain. It is likely that the infinite flow is unstable and the realization of the steady laminar Bödewadt flow in the laboratory may not be feasible. If one could construct a steady-rotating-flow apparatus where the fluid away from the disk is rotating faster than the disk, then the disk boundary layer would be turbulent. Flow structures developing at larger radii would eventually breakup while being convected toward the centre of the disk. The turbulent fluid would fill the boundary layer. One would not be able to see the evolution of the infinitesimal waves into large-amplitude waves and their subsequent breakdown to turbulence at a certain transition radius, for example, as in the flat-plate boundary layer or as in the Ekman boundary layer when the fluid away from the disk is rotating slower than the wall. A solution to this problem is to study the flow under unsteady conditions where there is some time available during which the evolution of the waves may be observed, however short that timespan may be. The experimental study presented here is one such case.

The topic of this article is an experimental investigation of the stability of the axially symmetric boundary layer due to the solid-body rotation of a fluid over a stationary disk. The partial differential equations for the steady flow may, by an appropriate similarity transformation, be reduced to a set of ordinary differential equations whose discovery and solution are due to Bödewadt (1940). The flow over the end disks in a cylindrical cavity during impulsive spin-down to rest closely approximates the Bödewadt flow. The preliminary results reported by Savaş (1983) of the flow visualizations in such a boundary-layer flow showed a new class of waves. They are circular, occur deep in the boundary layer, and move slowly toward the centre of the disk. The breakdown and transition to turbulence starts at the perimeter and progresses toward the centre. The present article is a detailed account of that experimental study.

2. Experimental set-up

2.1. *Apparatus*

Velocity measurements are made in toluene in the rotating-flow apparatus shown in figure 1(*a*). The set-up consists of a circular cylinder mounted on a turntable assembly. The cylinder is made out of Pyrex glass tubing. It has an internal diameter $2R$ of 21.7 cm. An aircraft-grade lucite disk is glued onto the cylinder. A nylon insert forms the bottom of the cavity. The height-to-diameter ratio of the cavity $H/2R$ is

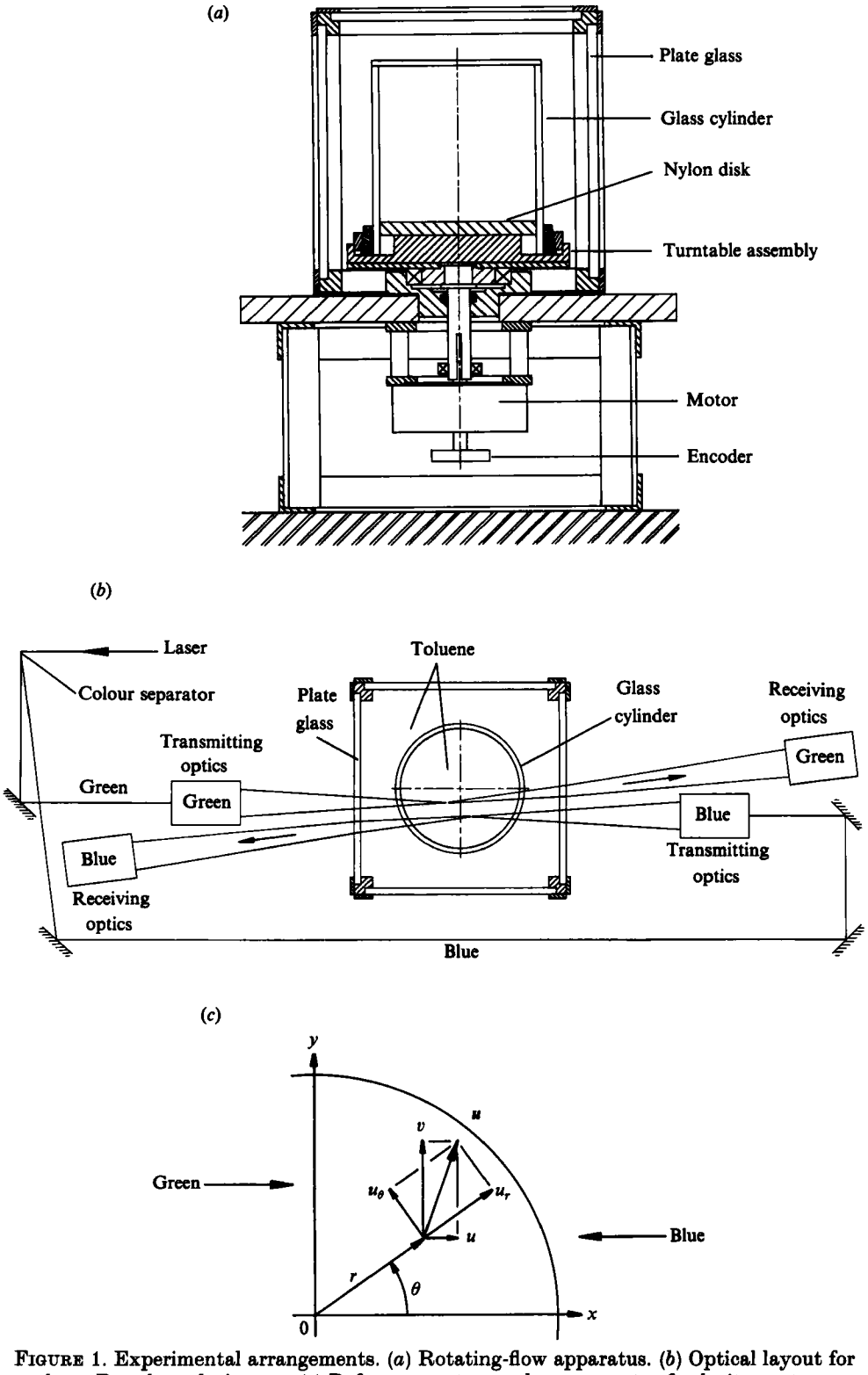

FIGURE 1. Experimental arrangements. (*a*) Rotating-flow apparatus. (*b*) Optical layout for laser-Doppler velocimetry. (*c*) Reference system and components of velocity vector.

1.0. The cylinder is clamped onto an aluminium base. This base is screwed to the turntable. The cylinder and the turntable are enclosed in a 40 cm cubical glass container. The walls of the cube are made of 1 cm thick plate glass. The cubical cavity is hermetically sealed both at the motor shaft and the glass sidewalls. The turntable is driven by a programmable servo amplifier. Constant speeds could be achieved within 0.2% of the set speed. Impulsive speed changes are implemented for the present experiments. The turntable assembly accelerates at a rate of 30 rad/s^2 and decelerates at a rate of 40 rad/s^2.

The working fluid is toluene (density $\rho = 0.87$ g/cm^3 and kinematic viscosity $\nu = 0.0067$ cm^2/s at 23 °C). The fluid fills the cylindrical cavity and that between the cylinder and the surrounding glass cube. The index of refraction of toluene is 1.494 and that of Pyrex glass 1.474. The close match of the indices alleviates the problems caused by the cylindrical surfaces during optical probing into the cavity. Further, the low kinematic viscosity of toluene permits relatively high Reynolds numbers $Re = r(\Omega/\nu)^{\frac{1}{2}}$ at low table speeds Ω [based on the local boundary-layer lengthscale $(\nu/\Omega)^{\frac{1}{2}}$ and the azimuthal component Ωr of the local velocity vector in the core]. The fluid is seeded with 2 μm diameter uniform glass microspheres for laser-Doppler velocimetry. The particle number density is about 10^6 cm^{-3}. The settling rate of a glass sphere is about 2 cm/hr. Velocity measurements in the boundary layer were made over the lower disk where the scattering-particle number density is higher than that over the upper disk due to the settling of the glass spheres under gravity.

2.2. *Velocimetry*

Velocity measurements are made with a laser-Doppler velocimeter system. The optical arrangement is shown in figure 1(*b*). This system has evolved from a commercially available unit (Thermal Systems Inc. Model 1990). The coherent light source is a fixed 2 W argon ion laser. The green (514.5 nm wavelength) and blue (488.0 nm wavelength) light beams from the laser are used for probing into the flow. The transmitting and the receiving optics for the green beam are stationary in the laboratory coordinate system. The blue-beam optics are placed on a two-dimensional traversing mechanism. This mechanism and its mirrors are so arranged that the blue optics can be positioned independently in the x- and y-directions (cf. figure 1*c*). Thus, the green and the blue optics can be positioned relative to each other in the z-plane. The turntable assembly is mounted on a three-dimensional traversing mechanism. The optical arrangement enables simultaneous velocity measurements at any two points in z-planes selected by the vertical position of the flow apparatus.

Two signal processors dedicated to the green and the blue beams are interfaced to a computer. The sampling rate is controlled by a preset counter. Time histories of the velocity signals are recorded by the data acquisition systems. A typical experiment starts after the cylinder assembly has been rotating at an initial constant speed Ω_i for about 30 min. Numerous preliminary runs indicated the necessity of such a long relaxation time for the inertial oscillations to subside and for the contents of the cylinder to reach solid-body rotation. The experiment is started by implementing a final constant rotation speed Ω_f or by stopping the cylinder. The time $t = 0$ mark from the servo amplifier starts the data acquisition. Sampling rates range from 10 to 200 Hz. The free-running data rates of the two signal processors are adjusted typically to two orders of magnitude higher than the sampling rate to make simultaneous measurements within an acceptable time window. The velocity traces presented in this article are digitally filtered off line to remove the high-frequency instrumentation noise. The filtering is done through the convolution of the velocity traces by a Gaussian window.

2.3. *Flow visualization*

Flow visualizations are done in water in the apparatus described by Savas (1983). A circular light source constructed of twenty-four incandescent frosty light bulbs is used as the illumination source for the aluminium flakes which act like minute mirrors in the flow field. The light circle has a diameter of 1 m and is placed 35 cm vertically above the cylinder. A camera placed along the axis of the cylinder has recorded the pictures shown in figure 2. A brief discussion of the appropriate lighting to visualize this axisymmetric flow is given by Savaş (1983). A quantitative discussion of the visualization technique may be found in Savaş (1985).

The usual Cartesian (x, y, z) and cylindrical (r, θ, z) coordinate systems are used (figure 1*c*). The origin is located at the centre of the bottom disk of the cylindrical cavity. The z-axis measures the distance from the surface of the disk and into the cavity. Thus, the mid-plane of the cavity is at $z = 10.9$ cm. The components of the velocity vector $\boldsymbol{u}$ are (u, v, w) in the (x, y, z)-directions and (u_r, u_θ, w) in the (r, θ, z)-directions.

3. Discussion

3.1. *Flow visualization*

The photographs in figure 2 show the disk boundary layer at various flow conditions. The observable depth in the pictures is about 1 cm. The low-Reynolds-number regimes exhibit the circular waves in isolation. The pictures in figure 2(*a*) shows these waves over the inner region of the disk. The initial rotation rate of the fluid was 1.55 rad/s before the cylinder was impulsively brought to rest. The waves are circular. They move toward the centre with a low phase velocity which decreases slightly as they approach the centre (Savaş 1983). The circular light source has axisymmetrically illuminated the boundary layer. No modulation due to the individual light bulbs is observable in the reflected light intensity from the aluminium flakes. The waves in the picture develop into azimuthal vortices. Therefore, two successive bands of bright or dark circles do not necessarily indicate one wavelength. They can also indicate rolled up material surfaces within one wavelength. No signs of boundary-layer separation are observable. The central region of the disk is calm. As the waves move into that region, their activity subsides. Evidently, the waves are moving into a stable region of the flow. This argument is plausible since the waves are moving into a region of the flow with lower Reynolds number. The Reynolds number $r(\Omega/\nu)^{\frac{1}{2}}$ is about 30 at the innermost circle in figure 2*a*. The dark spot at the centre of the disk is due to the alignment of the flakes parallel to the axis of the cylinder as the fluid leaves the boundary layer for the core. The fluid occupying the outer region of the disk adjacent to the cylindrical wall and characterized by the irregular patterns in the picture is mostly the debris convected from the cylindrical wall and partly the remnants of the earlier waves which have broken down. A series of photographs showing the evolution of the circular waves is given by Savaş (1983).

Figure 2(*b*) shows the boundary layer at a high Reynolds number shortly after the cylinder is brought to rest from $\Omega_i = 4.60$ rad/s. A higher instability mode, a spiral mode, occurs simultaneously with the circular waves. These spiral waves are at 12–18° toward the centre from the azimuthal flow direction. They are evidently the Type I (Class B) waves. Twenty-three cycles are present in this particular picture. Figure 2(*b*) clearly isolates the class of circular waves of figure 2(*a*) from the spiral Type I waves. At high rotation rates the deceleration time of the cylinder becomes

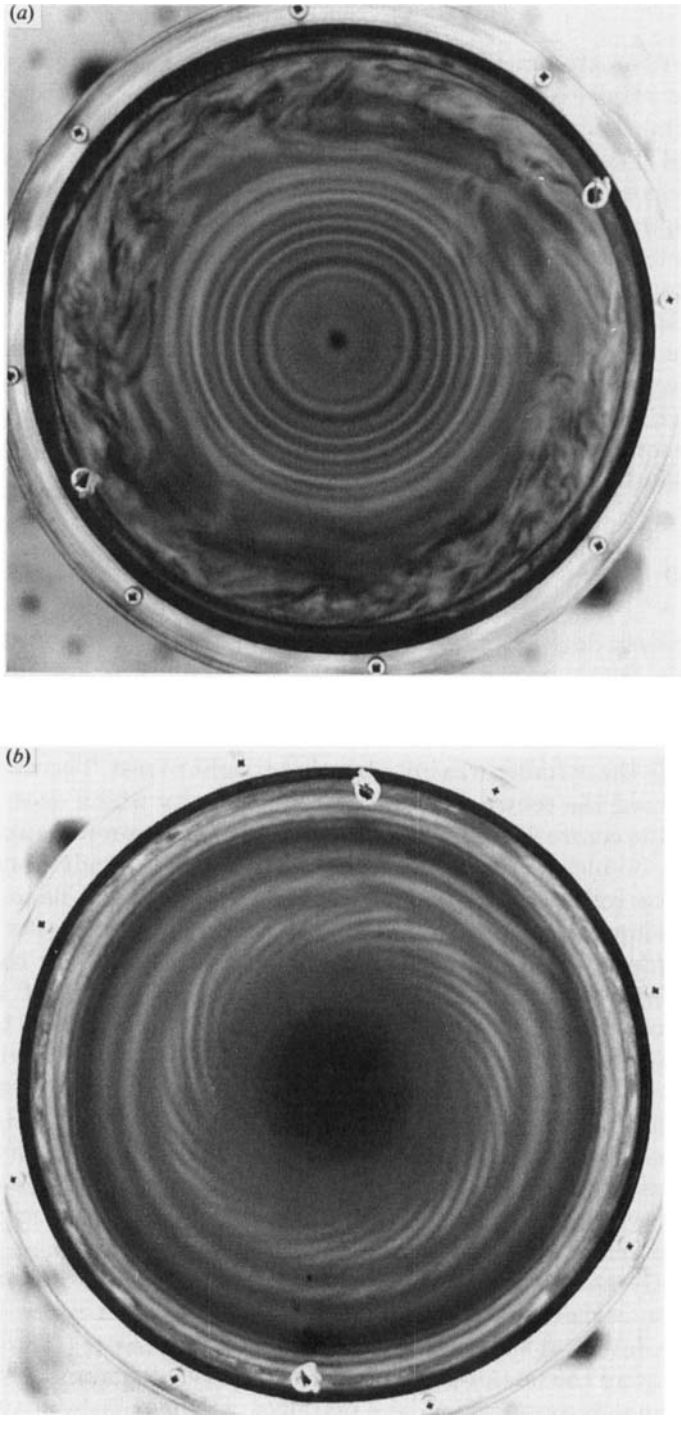

FIGURE 2 (*a*, *b*). For caption see facing page.

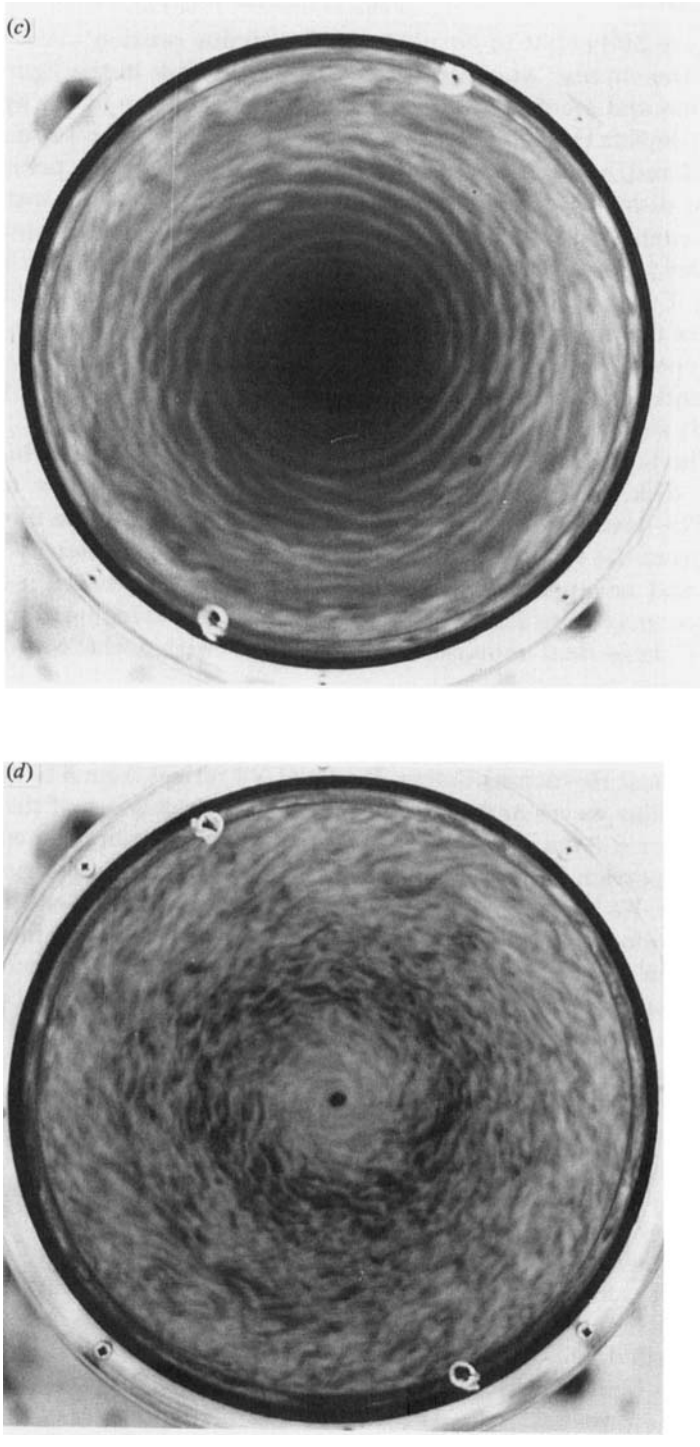

FIGURE 2. Flow visualization in water (counter-clockwise rotation). (*a*) Circular waves at low Reynolds number ($\Omega_i = 1.55$ rad/s); (*b*) circular waves and spiral waves (Type I, Class B) at high Reynolds number ($\Omega_i = 4.6$ rad/s); (*c*) circular waves and spiral waves (Type II, Class A) during nonlinear spin-down from $\Omega_i = 3.5$ to $\Omega_f = 1.7$ rad/s; (*d*) turbulent boundary layer ($\Omega_i = 6.3$ rad/s).

comparable with the evolution time of the boundary layer and with that of the waves; therefore, figure 2(*b*) ought to be interpreted with due caution. Also, the slight local distortion of the circular waves near the edge of the disk in the figure is repeatable at that location and seems to be due to a local imperfection in the apparatus.

Figure 2(*c*) depicts the boundary layer soon after the cylinder was impulsively spun down from 3.5 rad/s to 1.7 rad/s. Continuous circular waves are present in the inner region of the disk. That region is surrounded by intermittent waves with larger wavelengths compared to the Type I waves of figure 2(*b*). These intermittent waves are at 0–5° away from the centre with respect to the azimuthal flow direction. They are evidently Type II (Class A) waves. Hence, figure 2(*c*) clearly isolates further the circular waves from the Type II waves. Nevertheless, there remains the possibility that these Type II waves are a later stage in the development of the circular waves seen in the central region of the disk in figure 2(*c*) (cf. conclusions of Szeri *et al.* 1983).

Figure 2(*d*) shows the developed stage of the flow over the disk. It is evidently turbulent. The boundary layer exhibits an apparently uniform turbulent scale over most of the disk. No signs of separation are visible. The flow maintains axial symmetry. The dark spot at the centre is similar to that in figure 2(*a*) and indicates the outflow from the boundary layer at the centre. The persistently stable shape of that region and an apparent trend toward order at the centre indicate that the boundary layer may have a stabilizing effect in the central region of the disk. Further discussion of these final remarks is given below within the context of stability arguments.

3.2. *Velocity measurements*

The experiments cover the ranges of angular speeds of 0.13–3.5 rad/s and radii of 1–10 cm. The local Reynolds number $Re = r(\Omega/\nu)^{\frac{1}{2}}$ ranges from 5 to 230. The domain covers the circular waves and overlaps the spiral waves. Most of the measurements are confined to $r < 5$ cm in order to have enough time before the convected debris from the outer portion of the disk and the cylindrical wall is swept into the developing boundary layer. No hardware for shifting the frequencies of the laser light beams was available. Therefore, the radial velocity component u_r, which is in the direction of the wave motion and starts from zero, could not be reliably measured. The azimuthal velocity component u_θ is measured for detecting the waves in the transient flow. Modulations in the amplitude of the velocity histories are recorded that are due to the circular waves propagating toward the centre in the disk boundary layer.

Figure 3 shows sample measurements of the azimuthal velocity component under conditions comparable with those of the flows depicted in figure 2(*a*, *b*). All traces in figure 3 are recorded at $(r, z) = (4.5\text{ cm}, 4.0\text{ mm})$. A quiescent period following the impulsive spin-down is characteristic of all traces. Viscous diffusion dominates that phase of the flow. The wavy nature of the flow becomes apparent after the boundary layer adjusts itself to the new conditions. The waves are clearly recorded at low Reynolds number in figure 3(*a*). The probe is deep in the boundary layer at this low Reynolds number. As the waves roll into azimuthal vortices, a surface of discontinuity is recorded in the latter stages of the flow as indicated by an arrow in the figure (see also figure 5*a* below). Further, signs of breakup are also present in the figure. These slow oscillations near the centre are the signatures of the circular waves of figure 2(*a*). The traces in figure 3(*b*, *c*) recorded at higher Reynolds numbers contain finer details in addition to the large-amplitude, low-frequency circular waves. These additional features are due to the spiral Type I (Class B) waves. The noise level at these high flow velocities increases due to the lagging of the glass beads in toluene. The final phases of the flows become erratic quickly, owing, perhaps, to the fact

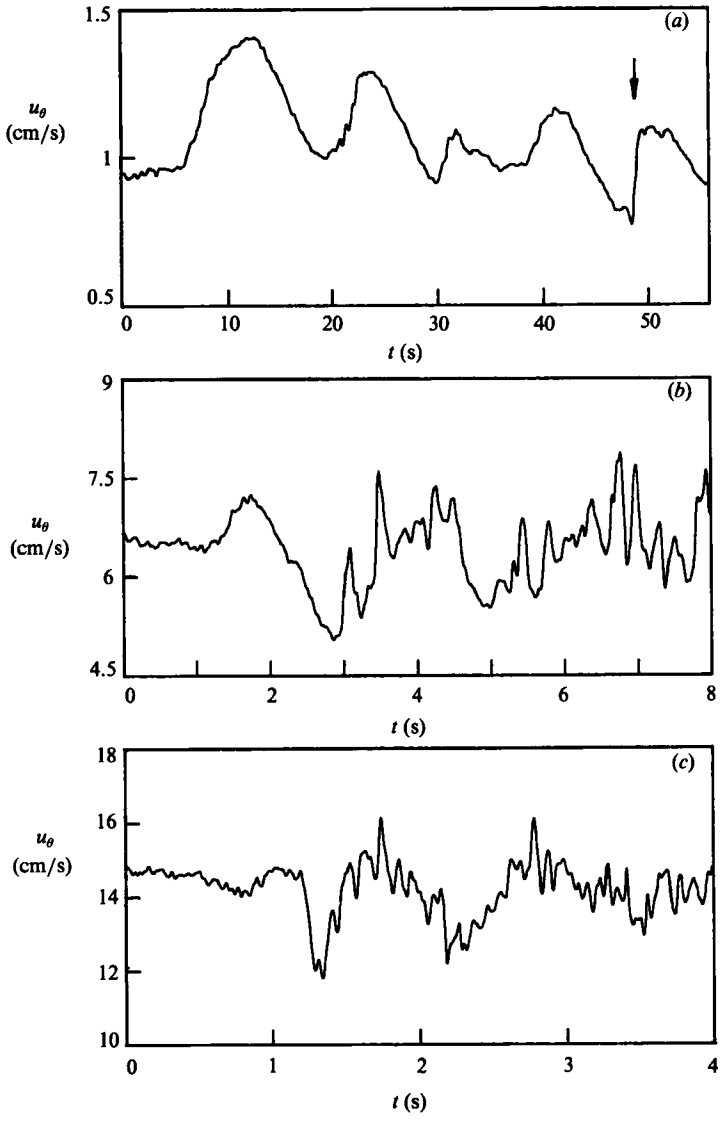

FIGURE 3. Sample velocity histories at $r = 4.5$ cm and $z = 4$ mm. (*a*) Low Reynolds number ($\Omega_1 = 0.21$ rad/s); (*b*) moderate Reynolds number ($\Omega_1 = 1.51$ rad/s); and (*c*) high Reynolds number ($\Omega_1 = 3.26$ rad/s).

that the boundary layer is already turbulent in the latter portions of the traces in figure 3 (*b*, *c*). These two traces are comparable with the picture of figure 2 (*b*) where the spiral waves of Type I are riding on the circular waves and extending alone toward the centre of the disk.

Figure 4 shows six velocity traces in the boundary layer at different radii. The traces are simultaneous in pairs. All traces are taken at $z = 4.5$ mm and at $\Omega_1 = 0.5$ rad/s, and therefore at $z(\nu/\Omega_1)^{\frac{1}{2}} = 3.9$, which lies at the outer edge of the Bödewadt boundary layer. The measured component of the velocity vector is v at $\theta = 45°$ (cf. figure 1*c*). The traces accentuate both the radial and the azimuthal fluctuations. The flow is incoherently fluctuating at the outer radii while the circular

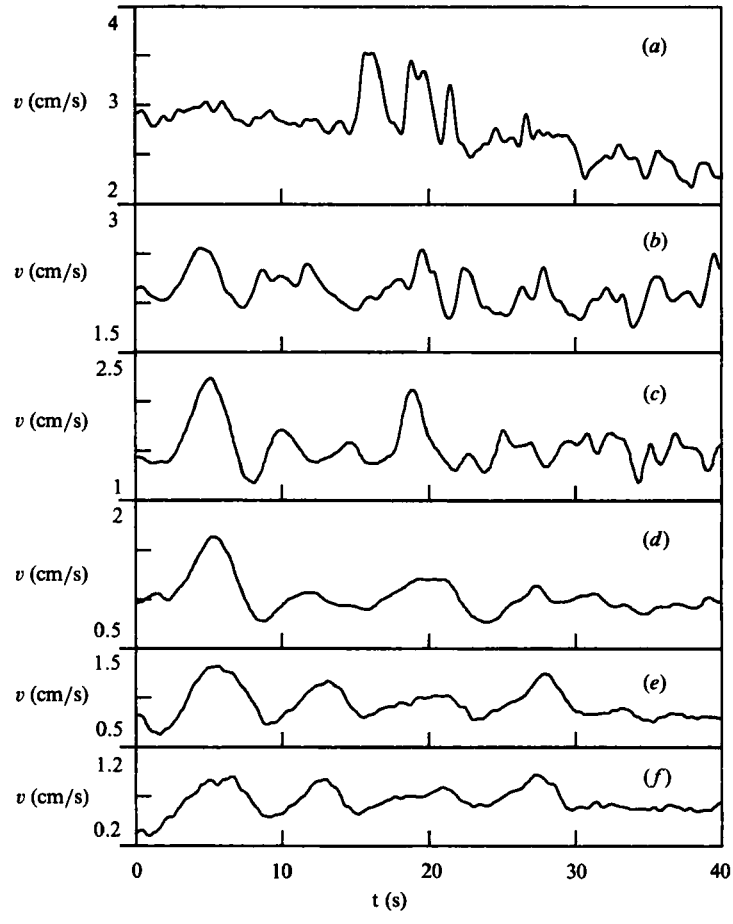

FIGURE 4. Velocity traces showing the nature of the flow over the disk during spin-down to rest ($\theta = 45°$, $z = 4.5$ mm, $\Omega_1 = 0.5$ rad/s). The traces are simulations in pairs of (a, b), (c, d) and (e, f). (a) $r = 8.0$ cm, (b) 5.6 cm, (c) 4.0 cm, (d) 2.8 cm, (e) 2.0 cm, and (f) 1.4 cm.

waves are evolving in the inner region of the disk. The initial response of the boundary layer is approximately the same over the disk and is characterized by an overshoot of the Bödewadt velocity profile at this depth (the response of the boundary layer is further discussed below). The waves breakdown earlier at the larger radii (cf. figure 4b, e).

The conspicuous high excursions on the simultaneous traces in figure 4(a, b) are due to the convected debris from the cylindrical wall. The flow during spindown is inherently unstable. The cylinderical wall (which is at rest in the case of spin-down to rest) and the faster rotating core away from the concave surface are conductive to the Taylor instability mechanism, much like the circular Couette flow when the inner cylinder is rotating faster than the outer one. Soon after the speed of the cylinder is reduced, the flow in the vicinity of the cylinder becomes unstable and Taylor–Görtler vortices develop. These vortices are observed during the flow-visualization experiments. The flow pattern in the cylinder during spin-down is such that these vortices are convected toward the end disks of the cavity (cf. figure 2a). The traces in figure 4(a, b) show velocities recorded in the vicinity of the corner where the convected vortices should be encountered without much distortion. The traces in

figure 4(*e*, *f*) are closer to the centre in the disk boundary layer where the circular waves are present. The traces of figure 4(*a*, *b*) show a convective process occurring near the cylinderical wall while the interior of the disk is experiencing a locally originated wave activity. In another series of experiments, the deceleration of the cylinder was varied from 2.5 to 40 rad²/s. The wave behaviour as indicated by the velocity measurements did not differ substantially from that described above.

3.3. *Development of the boundary layer*

The evolution of the boundary-layer flow is shown in figure 5 at $r = 5.1$ cm following the impulsive spin-down to rest from $\Omega_i = 1.0$ rad/s. The profiles in figure 5(*b*) of the azimuthal velocity component are constructed from single time histories recorded at various distances from the wall, such as the traces shown in figure 5(*a*). Values corresponding to time-steps are extracted from the traces through a Gaussian filter. The velocity component u_θ is scaled with the instantaneous angular velocity $\Omega(t)$ of the core, which is determined as described below. The individual values are adjusted for the inadvertent variations in the initial rotation speed Ω_i. The numerical solution of the steady-state velocity profile in the Bödewadt flow is also shown for comparison at each instant. The profile is initially uniform except for the impulsive diffusive behaviour in the vicinity of the wall. The boundary layer responds simultaneously across its depth. Following an overshoot in the region 2 mm $< z <$ 6 mm, the profile settles approximately to the steady-state solution after about 4 s, or equivalently, 4 rad rotation of the core at $\Omega_i = 1.0$ rad/s. The instability waves dominate the flow thereafter and the profiles lose their coherence. The waves are confined to the boundary layer as indicated by the traces in figure 5(*a*) and profiles in figure 5(*b*). Figure 5(*c*) shows the velocity profile constructed by averaging the transient velocity records over the timespan of the waves, which is about 5 s at $\Omega_i = 1.0$ rad/s. The result is in good agreement with the steady profile in spite of the high modulation in the velocity traces. Therefore, a stability analysis of the Bödewadt flow, using as the background flow the laminar solution of the steady-flow equations, should theoretically confirm the circular waves. A similar profile constructed after the flow in the boundary layer becomes turbulent is shown in figure 5(*d*) (cf. figure 2*d*). Even though the turbulent Bödewadt flow has not been studied, the data of figure 5(*d*) indicate a similarity with its laminar counterpart.

3.4. *Response time*

The flow studied here is unsteady at numerous levels. The first distinction may be made with regard to the various instabilities present in the flow such as inertial oscillations and Taylor–Görtler vortices. Those aspects of the flow are beyond the scope of this article. The formation of the boundary layers over the end disks and the subsequent transient motion of the core, which is primarily a result of the secondary flows induced in the two quasi-steady disk boundary layers, are closely related to the subject matter of this article. Figures 6(*a* and *b*) compare the response of the core and the disk boundary layer to the impulsive speed change during spin-down to rest. A sample velocity history of the core is shown in figure 6(*a*). The flow is characterized by intense fluctuations in a monotonically slowing mean flow. The nature of these fluctuations need not be considered here. The mean flow of the inviscid core can be modelled by using vortex stretching arguments. The model matches the uniform axial velocity at the ends of the cylindrical core to the uniform ejection velocity of the end-disk boundary layers. The angular velocity of the core in solid-body rotation can be expressed by the simple expression $\Omega(t)/\Omega_i = (1+\tau)^{-2}$,

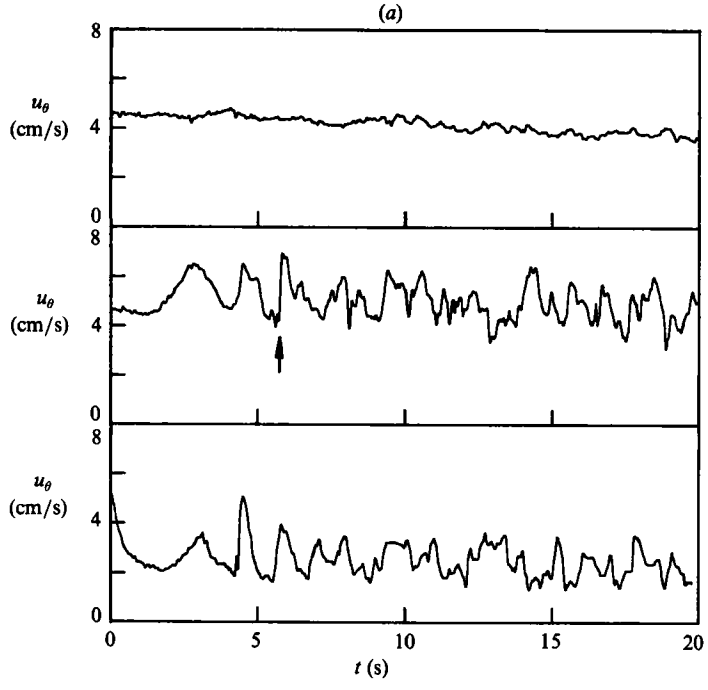

FIGURE 5(a). For caption see facing page.

where $\tau = 0.69(2R/H)(\nu/\Omega_1 R^2)^{\frac{1}{2}}\Omega_1 t$ (Weidman 1976). The prediction of this model is also shown in figure 6(a) by a smooth curve over the measured velocity history. The model describes well the average behaviour of the core. Hence, the mean behaviour of the angular velocity of the core $\Omega(t)$ given by the expression above is used in the discussions in this article (e.g. figure 5). Figure 6(b) shows the velocity history recorded in the Bödewadt boundary layer simultaneously with that in the core shown in figure 6(a). The azimuthal velocity component overshoots and returns to a quasi-steady state except for the waves. The response time T of the boundary layer is taken, as shown in figure 6(b), to be the time interval between the implementation of the impulsive speed-change command and the occurrence of a characteristic signature observed in the boundary layer (cf. figures 4 and 5). Such a signature is clearly identifiable in the outer region of the boundary layer (cf. figure 4). The results are summarized in figure 6(c). The decrease in the angular velocity of the core during the adjustment period of the boundary layer is small and, hence, the response time T is normalized with the initial rotation rate Ω_1 of the cylinder. The core fluid travels about 4 rad in the time that it takes the boundary layer to reach its quasi-steady state. This is in agreement with Benton's (1966) numerical calculations of the evolution of boundary layers over rotating disks.

3.5. *Inertial oscillations*

Impulsive changes in the speed of the container excite the inertial oscillations in the core of the cylinder. The linear oscillations that occur when the speed changes are small have been analysed analytically and verified experimentally (see, for example, Greenspan 1968). The nonlinear counterparts of these oscillations occur during the large impulsive changes in the speed of the container. The frequencies of individual

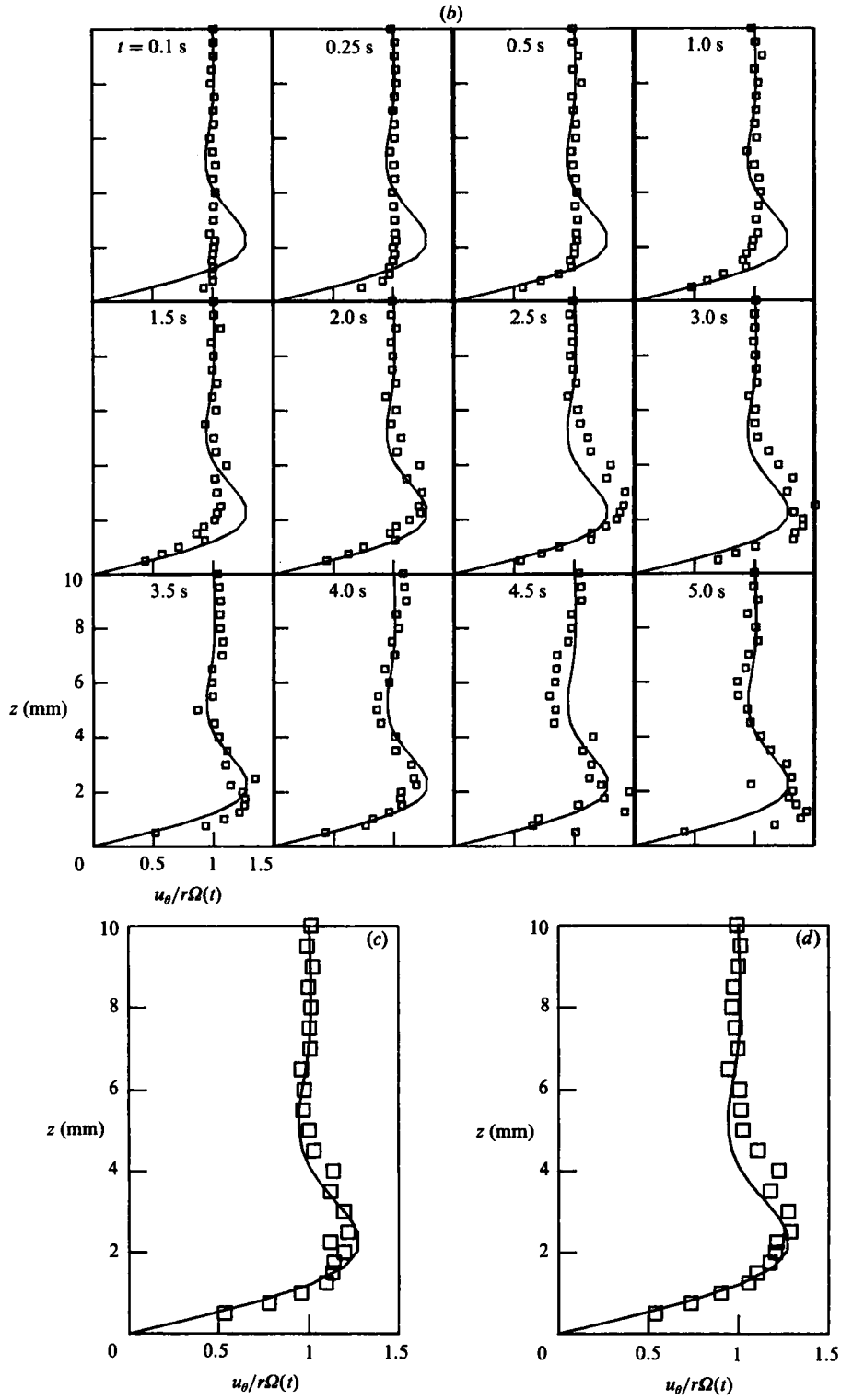

FIGURE 5. Evolution of the boundary layer during spin-down to rest (average $\Omega_1 = 1.0$ rad/s and $r = 5.1$ cm). (*a*) Velocity traces at $z = 10$ mm (top), $z = 2$ mm (middle), and $z = 0.5$ mm (bottom). (*b*) Evolving Bödewadt flow: □, measurements; ——, Bödewadt's solution (also in *c* and *d*). (*c*) Average profile during the wave activity. (*d*) Average profile in turbulent regime.

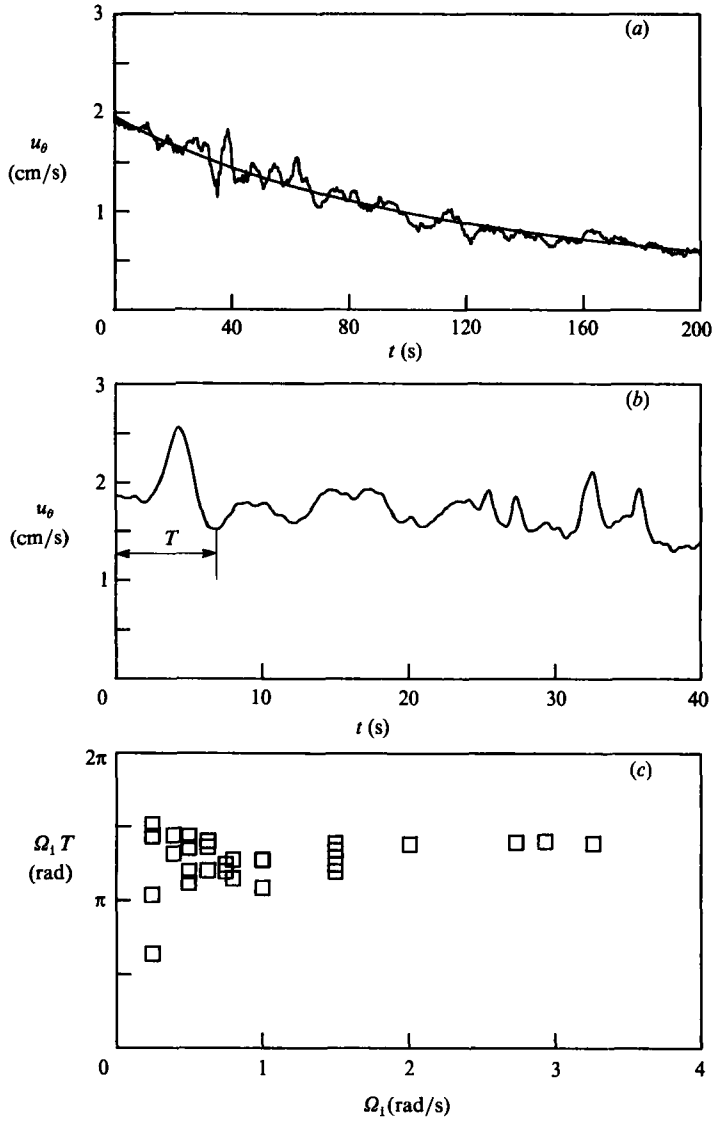

FIGURE 6. Response of the flow during spin-down to rest ($\Omega_i = 0.64$ rad/s and $r = 3.1$ cm). (*a*) Sample velocity history in the core ($z = 10.7$ cm). Smooth curve after Weidman (1976). (*b*) Sample velocity history in the boundary layer ($z = 4$ mm) taken simultaneously with the trace in (*a*). (*c*) Response time $\Omega_i T$ of the boundary layer as defined in (*b*) versus the initial rotation rate Ω_i.

modes may be somewhat different from those of the linear oscillation modes. The oscillations may excite the boundary layers. That the circular waves are not manifestations of the inertial oscillation modes of the cylinder is demonstrated in figures 4–7. The boundary layer does not oscillate uniformly in figure 4. The wave activity is confined to the boundary layer as shown by the measurements in figure 5 (*a*). The simultaneous traces in figure 6 (*a*, *b*) show a sample experiment where one of the velocity probes is located at the mid-plane of the cylinder and the other in the boundary layer. The boundary-layer probe is recording the circular waves which have

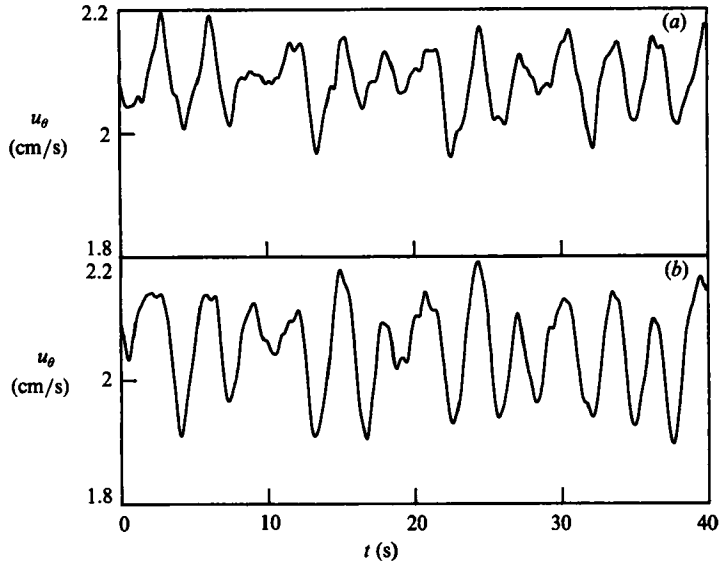

FIGURE 7. Inertial oscillations: simultaneous velocity measurements (*a*) in the mid-plane ($r = 3.1$ cm and $z = 10.7$ cm and (*b*) in the boundary layer ($r = 3.0$ cm and $z = 5$ mm) during self-excited inertial oscillations within the cylinder rotating steadily at 0.68 rad/s.

large amplitudes while the mid-plane probe does not show a comparable behaviour. Figure 7 (*a*, *b*) displays simultaneous velocity histories recorded at the two probes when the cylinder is rotating steadily at 0.68 rad/s and inertial oscillations are present. In this arrangement, as in figure 6 (*a*, *b*), one probe is at the edge of the disk boundary layer and the other is at the mid-plane of the cylinder and vertically above the first one. The container speed is not modulated. The oscillations are excited following an earlier modulation of the cylinder. The two traces are well correlated as expected for the oscillations. In this particular case, the velocities are in phase and have comparable amplitude modulations. Hence, the inertial oscillation modes of the cylinder do not play a significant direct role in the development of the circular waves in the Bödewadt boundary layer.

4. Stability

Figure 8 shows the measured stability characteristics of the Bödewadt flow and is the main result of this article. The scaling is after that of the flat-plate boundary layer except for the lengthscale, where $(\nu/\Omega_1)^{\frac{1}{2}}$ is used.

Figure 8 (*a*) shows the wavenumber $2\pi/\lambda$ of the circular waves versus the local Reynolds number $r(\Omega/\nu)^{\frac{1}{2}}$. The data in the figure are obtained from pictures and replotted from Savaş (1983). The data suggest a critical Reynolds number of about 30. This value should be taken as an upper limit for the critical Reynolds number of the Bödewadt boundary layer. The inflow from the edges of the disk and waves that move toward the centre encounter a stable region during their journey. That should suppress the fluctuations and force stabilization. The relative calmness of the flow in the central part of the disk was a conspicuous feature of all flow-visualization observations. Evidence of this calmness is provided in figure 2 (*a*), where the central

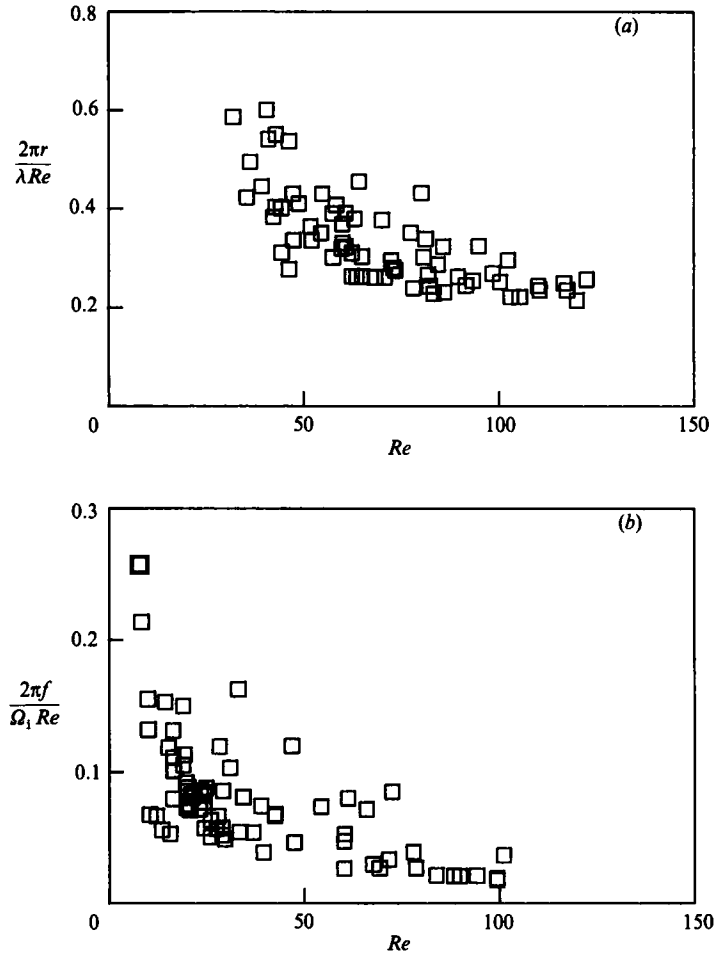

FIGURE 8. Stability diagrams: (*a*) wavenumber $2\pi r/\lambda Re$ and (*b*) frequency $2\pi f/\Omega_1 Re$ as functions of the local Reynolds number $r(\Omega_1/\nu)^{\frac{1}{2}}$.

part of the disk is free of wave activity. Further evidence is present in figure 2(*d*). The turbulent boundary layer loses its incoherence as the fluid approaches the centre. Eventually, the fluid leaves the disk in an orderly manner as evidenced by the rather smooth boundary of the central dark spot (cf. figure 2*a*).

The measured frequencies of the circular waves are shown in figure 8(*b*). The data are extracted from velocity traces such as those shown in figures 3–6. The frequency f is scaled with $\Omega_1 r$, which approximates the local azimuthal velocity in the core during the wave activity. Since the waves move toward the centre as they develop, an upper envelope to the data in the figure should be taken as the stability limit. The figure indicates a critical Reynolds number of about 20, which is smaller than that indicated in figure 8(*a*). That may be attributed to the fact that the waves move toward the centre where the background flow becomes stable. The wave activity that is being convected from the unstable region of the disk will still register oscillations in the velocity measurements. Therefore, the critical Reynolds number implied in figure 8(*b*) ought to be taken as a lower bound. When the two bounds indicated in figure 8 are considered together, then one may conclude the critical Reynolds number

for the circular waves to be about 25. The corresponding critical dimensionless wavenumber $2\pi r/\lambda Re$ is about 0.6 and the dimensionless frequency $2\pi f/\Omega_i Re$ about 0.2.

5. Closing remarks

The behaviour of the flow over the disk in a cylindrical cavity during spin-down to rest is studied experimentally. The temporal evolution of the boundary-layer profile is determined from the measurements of the azimuthal component of the velocity vector. The flow approximates that described by Bödewadt. The core fluid travels about 4 rad during the evolution of the disk boundary layer. Observations and measurements made in the boundary layer show that a class of circular waves is excited. The average disk-boundary-layer profile during the lifespan of these circular waves remains similar to the steady profile of the Bödewadt flow. Therefore, a stability analysis of the Bödewadt flow would be germane to the understanding of the class of waves observed in this study. At sufficiently high Reynolds numbers, the Type I spiral waves are also excited along with the circular waves. The number of the circular-wave cycles seems to be restricted by the size of the disk. This is evident in figure 2(*b*) where barely two cycles of the circular waves are observable at that rotation rate. A larger disk may alleviate that problem. However, the flow is likely to rapidly become locally turbulent at larger radii and the inward convection of the fluid will eventually render the boundary layer turbulent. The average-velocity profile remains similar to its laminar counterpart after the boundary layer becomes turbulent.

I thank Martin C. Jischke for his contributions to the fluid mechanics laboratory. I have benefitted from discussions with Donald Coles and John M. Russell.

REFERENCES

BENTON, E. R. 1966 On the flow due to a rotating disk. *J. Fluid Mech.* **24**, 781–800.

BÖDEWADT, U. T. 1940 Die Drehströmung über festem Grunde. *Z. Angew. Math. Mech.* **20**, 241–245.

CLARKSON, M. H., CHIN, S. C. & SHACTER, P. 1980 Visualization of instabilities on a rotating disk. *AIAA J.* **18**, 1541–1543.

DIJKSTRA, D. & HEIJST, G. J. F. VAN 1983 The flow between two finite rotating disks enclosed by a cylinder. *J. Fluid Mech.* **128**, 123–154.

FALLER, A. J. 1963 An experimental study of the instability of the laminar Ekman boundary layer. *J. Fluid Mech.* **15**, 560–576.

FALLER, A. J. & KAYLOR, R. E. 1966 Investigations of stability and transition in rotating boundary layers. In *Dynamics of Fluids and Plasmas* (ed. S. I. Pai), pp. 239–255. Academic.

FALLER, A. J. & KAYLOR, R. E. 1967 Instability of the Ekman spiral with applications to the planetary boundary layers. *Phys. Fluids Suppl.* **10**, S212–S219.

GREENSPAN, H. P. 1968 *The Theory of Rotating Fluids.* Cambridge University Press.

GREGORY, H. N., STUART, J. T. & WALKER, W. S. 1955 On the stability of three dimensional boundary layers with application to the flow due to a rotating disk. *Phil. Trans. R. Soc. Lond.* A **248**, 155–199.

KÁRMÁN, TH. VON 1921 Über laminare und turbulente Reibung. *Z. Angew. Math. Mech.* **1**, 233–252.

KEGELMAN, J. T., NELSON, R. C. & MUELLER, T. J. 1983 The boundary layer on an axisymmetric body with and without spin. *AIAA J.* **21**, 1485–1491.

KOBAYASHI, R. & IZUMI, H. 1983 Boundary-layer transition on a rotating cone in still fluid. *J. Fluid Mech.* **127**, 353–364.

KOBAYASHI, R., KOHAMA, Y. & KUROSAWA, M. 1983 Boundary-layer transition on a rotating cone in axial flow. *J. Fluid Mech.* **127**, 341–352.

KOHAMA, Y. 1985 Flow structures formed by axisymmetric spinning bodies. *AAIA J.* **23**, 1445–1447.

KOHAMA, Y. & KOBAYASHI, R. 1983 Boundary-layer transition and the behaviour of spiral vortices on rotating spheres. *J. Fluid Mech.* **137**, 153–164.

LENTINI, M. & KELLER, H. B. 1980 The von Kármán swirling flows. *SIAM J. Appl. Maths* **38**, 52–63.

ROGERS, M. N. & LANCE, G. L. 1960 The rotationally symmetric flow of a viscous fluid in the presence of an infinite disk. *J. Fluid Mech.* **7**, 617–631.

SAVAŞ, Ö. 1983 Circular waves on a stationary disk in rotating flow. *Phys. Fluids* **26**, 3445–3448.

SAVAŞ, Ö. 1985 On the flow visualization using reflective flakes. *J. Fluid Mech.* **152**, 235–248.

SZERI, A. Z., GIRON, A., SCHNEIDER, S. J. & KAUFMAN, H. N. 1983 Flow between rotating disks. Part 2. Stability. *J. Fluid Mech.* **134**, 133–154.

TATRO, P. R. & MOLLO-CHRISTENSEN, E. L. 1967 Experiments on Ekman layer stability. *J. Fluid Mech.* **28**, 531–543.

WEIDMAN, P. D. 1976 On the spin-up and spin-down of a rotating fluid. Part 1. Extending the Wedemeyer model. *J. Fluid Mech.* **77**, 685–708.

WILKINSON, S. P. & MALIK, M. R. 1985 Stability experiments in the flow over a rotating disk. *AIAA J.* **23**, 588–595.

ZANDBERGEN, P. J. & DIJKSTRA, D. 1977 Non-unique solutions of the Navier–Stokes equations for the Kármán swirling flow. *J. Engng Maths* **11**, 167–188.